A Method for Measuring In-Plane Forming Limit Curves using 2D Digital Image Correlation

Akshat Agha*, FADI Abu-Farha

[1]*FADI-AMT LLC, Greenville, SC, USA*
** Corresponding Author. Tel +1 (336) 346 4213; E-mail: akshat@fadi-amt.com*
ORCiD 0000-0001-9992-1114

Accepted in the SAE International Journal of Materials and Manufacturing (SAE-JMM) on March 7, 2023

ABSTRACT

With the introduction of advanced lightweight materials with complex microstructures and behaviors, more focus is put on the accurate determination of their forming limits, and that can only be possible through experiments, as the conventional theoretical models for forming limiting curve (FLC) prediction fail to perform. Despite that, CAE engineers, designers, and tool makers still rely heavily on theoretical models due to the steep costs associated with formability testing, including mechanical setup, a large number of tests, and the cost of a stereo digital image correlation (DIC) system. The International Standard ISO 12004-2:2021 recommends using a stereo DIC system for formability testing since 2D DIC systems are considered incapable of producing reliable strains due to errors associated with out-of-plane motion and deformation. This work challenges that notion and proposes a simple strain compensation method for the determination of FLCs using a low-cost single camera (2D) DIC system. In this study, formability tests are performed on an automotive-grade 6xxx series aluminum alloy using the Marciniak in-plane FLC testing method. The tests are performed on a custom setup that enables simultaneous optical strain measurements using a stereo DIC as well as a 2D DIC system. The results show how 2D DIC FLC points match those obtained by stereo DIC using two popular FLC approaches: ISO 12004-2 section-based spatial method and a time-dependent Linear Best Fit (LBF) method.

KEYWORDS

Full-field Strains, Digital Image Correlation, Forming Limit Curve, Sheet Metal Forming, Advanced High Strength Steels, Aluminum Alloys

1. INTRODUCTION

Forming limit curves (FLCs) and diagrams (FLDs) of sheet metal alloys are essential tools for the sheet metal forming industry, which aid in the design of new components and stamping dies. An FLD provides a measure for the stretchability of a material under various loading conditions, ranging from uniaxial tension to balanced-biaxial stretching. The FLD schematic shown in Figure 1 is a collection of strain pair clouds (major strain ϵ_1, minor strain ϵ_2) which are classified into safe, marginal, and failure regions. The key component of an FLD is the forming limit curve or FLC that defines the locus of the instable necking limit i.e., the red line in the plot. FLC is determined either theoretically or experimentally. Theoretical and empirically derived FLCs were first introduced by Keeler and Goodwin [1], [2] and later expanded by many other researchers. However, theoretical predictions of material formability are limited only to certain classes of materials, traditional steels in particular. With the introduction of several classes of advanced high-strength steels and new generations of aluminum alloys into the automotive body sector, traditionally FLC predictions are not capable of accurately capturing the complex formability response of these materials.

Experimental FLCs are generated by mechanical tests, the most popular of which are Marciniak in-plane

stretching tests [3] and Nakajima ball punch stretching tests [4]. Over the years, these mechanical tests have been coupled with several strain measurement techniques for instable necking detection. The most popular technique for strain measurement was the circle grid analysis used in combination with the finger touch method for necking detection [5]. The introduction of optical metrology, especially digital image correlation (DIC) for material testing has revolutionized modern-day testing approaches and enabled accurate strain measurements for previously impossible, complex testing scenarios and finite element validation [6]–[10]. The use of DIC, in particular, for forming limit evaluation has helped in the standardization of FLC testing methods. The integration of DIC in formability testing provides the strain history on the surface of the test sample deformed until rupture, which can be post-processed to determine the necking limits.

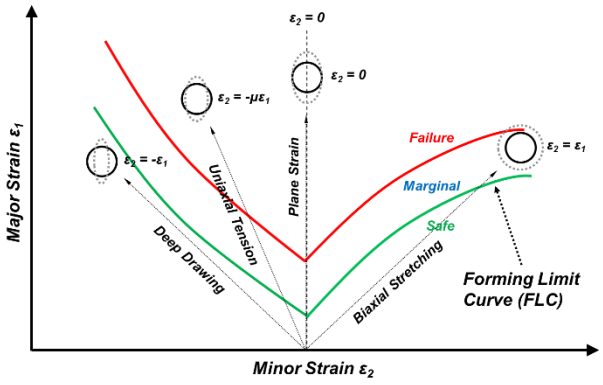

Figure 1. Schematic of a Forming Limit Diagram showing curves and loading conditions, taken from Ref. [11]

There are several methods published in the literature to determine the onset of instable necking from DIC computed strain pairs on a formability test sample. The FLC evaluation methods can be broadly divided into three categories – spatial methods (like ISO 12004-2:2021 section-based method [12]), temporal or time-dependent methods (like second derivative approach [13], Linear Best Fit method [14], [15], correlation coefficient approach [16]) and Spatio-temporal hybrid methods (curvature assisted necking zone approaches [17]–[19]). A detailed description and comparison of different approaches are presented by Hotz et al. [15], Min et al.[20] and Huang et al.[5].

Most formability tests involve out-of-plane deformation in the test sample, hence stereo DIC has always been the obvious choice for performing such tests. In fact, some researchers have even used multi-camera (N>2) DIC systems [5], [21] to increase the accuracy of FLC measurements. Despite the great benefits of a stereo DIC for formability testing, the biggest problem hindering its mass penetration is the high cost of commercial stereo DIC systems, which remains a substantially big investment, especially for academic institutions. To the best knowledge of the authors, formability testing is popularly done with a stereo DIC, and no published literature has shown the application of a single camera (2D) DIC system for formability testing since 2D DIC measurements are prone to errors associated with the out-of-plane translation of the test sample or the camera. In this light, if there is a way to overcome the errors associated with out-of-plane translation in a 2D DIC measurement, it can pose a viable and low-cost solution for formability testing. It will also serve as an efficient solution for the determination of forming limits at high strain rates, which is lately attracting a lot of attention from researchers [22], [23]. This paper is targeted towards bridging that gap, as it proposes a simple method of strain compensation for forming limit curves determination using a 2D DIC system.

Over the years, researchers have proposed several solutions to minimize/compensate for the errors and improve the accuracy of 2D DIC measurements for certain applications either mathematically or by using telecentric lenses [24]–[26]. In a previous publication, Agha [27] evaluated the effectiveness of 2D DIC in measuring fracture strains on sheet metal alloys and proposed a strain compensation method to reliably measure the fracture strains even for out-of-plane balanced biaxial tests. This paper builds on that work and expands into the formability testing of sheet metal alloys. In this work, formability tests using the Marciniak method are performed on a popular automotive-grade aluminum alloy using a custom test setup that enables simultaneous optical measurements using a stereo DIC and a 2D DIC system. The FLCs are generated using two popular approaches: (i) ISO 12004-2 section-based spatial method; (ii) time-dependent Linear Best Fit (LBF) method. Finally, the FLCs generated using the strain compensation method on 2D DIC measurements are validated against the benchmark FLCs generated by the stereo DIC measurements.

2. MATERIAL AND METHOD

2.1. Material

The aluminum alloy AL6 (Mg-Si based 6000 series aluminum alloy) of nominal thickness 1.0 mm was chosen to demonstrate the method proposed in this study. This aluminum alloy is predominantly used for making stamped outer body components for automotive vehicles. The mechanical properties of AL6 material are obtained through uniaxial tension tests performed using ISO 6892-Method B standard, and the engineering stress-strain curves of the material are plotted in Figure 2.

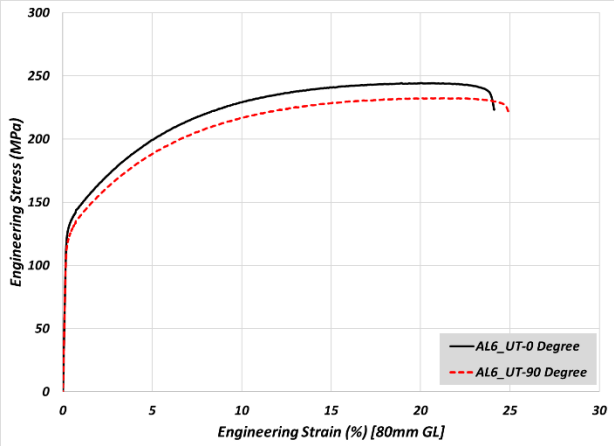

Figure 2. Uniaxial Tension Stress-Strain curves of AL6 aluminum alloy (1.0 mm thick)

2.2. Experimental Setup

The experimental test setup consists of a custom-built servo-hydraulic press (ITC SP400) with a clamping (binder) capacity of 1800 kN and a punch capacity of 1000 kN. The top plate of the press has a circular cut-out to enable the DIC cameras to view the test sample during testing. The 2D DIC and stereo DIC cameras are mounted on the top of the press as shown in Figure 3. The 2D DIC with custom hardware (utilizing an 8-megapixel CMOS camera with the appropriate optics) is set up to view the test sample normally, while the stereo DIC is a commercial 6-megapixel system. More details about the DIC calibration are given in Section 2.4.

The FLC tests were conducted using the Marciniak method, following the ISO 12004-2 standard. The Marciniak method provides uniform, nearly in-plane deformation in the center of the test sample [5], [20]. The test samples were clamped using 600 kN binder force before being deformed with a flat cylindrical punch (4" diameter) moving at 0.5 mm/s.

The two camera systems were programmed to receive a digital signal in order to auto-trigger at the start of the test; this enabled perfect synchronization between the two DIC systems.

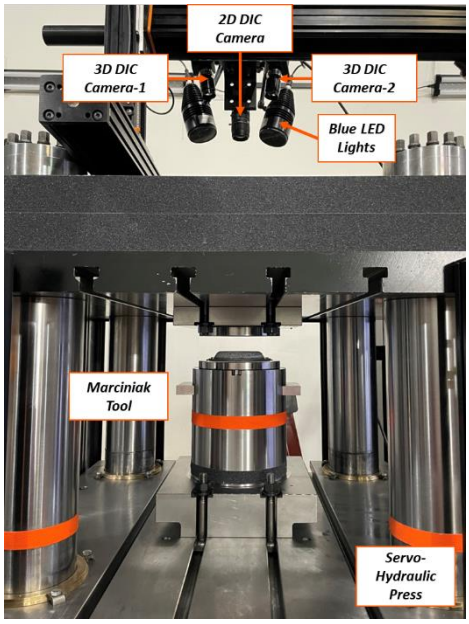

Figure 3. Test setup for FLC testing showing a servo-hydraulic press equipped with a top-mounted combined 2D and stereo DIC system

2.3. Test Samples Geometries

The Marciniak tests were performed on at least 7 different geometries to cover the entire FLC range from uniaxial tension to balanced biaxial stretching, as shown in Figure 4. At least three repeats were performed per geometry to ensure the repeatability of the test results. The samples were prepared by waterjet cutting so that the gage region is directed along the rolling direction of the sheet material. A mild steel carrier blank with a center hole was used between the test sample and the punch to enable friction-free and uniform stretching in the center of the test sample. Regular paints were used to generate the black-and-white speckle patterns needed for DIC tracking.

2.4. DIC Setup

The calibration of the stereo DIC system was performed per the manufacturer's instructions to ensure a calibration deviation of less than 0.05 pixels. The calibration of the custom 2D DIC system was simply done using a single image of a ruler held at the plane of the undeformed sample. The parameters critical to DIC measurements are given in Table 1 and explained in the following sections.

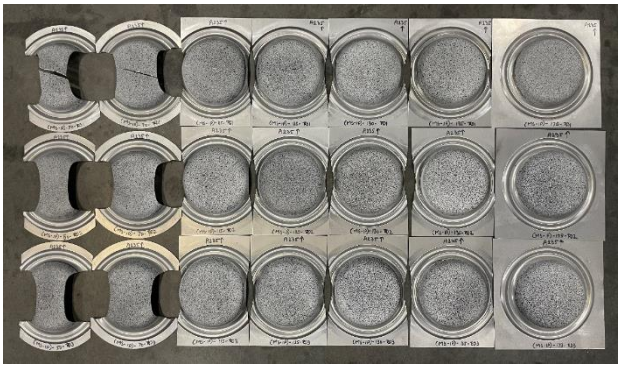

Figure 4. Tested Marciniak test samples of AL6 aluminum alloy

2.4.1. Pixel Resolution

The spatial resolution of the DIC measurements, given in microns per pixel, is the connection between the physical length in the field of view and the number of pixels. It was essential that the two systems used in this investigation have a similar spatial resolution, and this was ensured by carefully selecting the camera optics of the two systems. The 2D DIC and the stereo DIC setups generated 49 and 45 microns/pixel spatial resolutions, respectively; these values are close enough to compare the strain results obtained from the two systems.

2.4.2. Acquisition Frame Rate

The ISO 12004-2 standard recommends a minimum camera frame rate of 10 frames per mm of punch displacement, i.e., at least 5 Hz for the test speed of 0.5 mm/s. The chosen frame rate for this study was 20 Hz for the two DIC systems. The synchronized auto-trigger and the matching camera frame rate settings enabled the acquisition of images at the same timestamp and hence a one-to-one comparison of the results.

2.4.3. Virtual Strain Gauge Length (VSGL)

Another important parameter that affects strain calculations and thus DIC results, in general, is the chosen virtual strain gauge length. The point distance used in DIC computation generates a mesh of discrete points. The DIC computed strains are a function of the VSGL, interpolation scheme, and filtering window (neighborhood). In this study, the captured images (from both systems) were processed using the same commercial DIC software; the processing parameters (mainly the subset size and spacing) were chosen to produce a VSGL of ~1 mm. Moreover, strain interpolation and neighborhood averaging were matched, as shown in the Table 1.

Table 1. Optical System Details and DIC Processing Parameters

	Stereo DIC System	***2D DIC System***
System Type	Commercial	Custom-Built
Cameras	2 x 6 MP	1 x 8 MP
Lenses	50 mm	35mm
Lighting	Blue LED	Blue LED
Frame Rate (Hz) [used for testing]	20	20
Resolution (pixels x pixels)	2752x2200	2840x2840
Measuring Distance Z (mm)	~550	~450
Pixel Resolution (microns/pixel)	~45	~49
Facet Size (pixels)	43x43	43x43
Point Distance (pixels)	12	11
Virtual Gauge Length (mm)	~1	~1
Interpolation	Bicubic	Bicubic
Facet Matching	Against Ref. Frame	Against Ref. Frame
DIC Software Used	GOM Correlate Professional	GOM Correlate Professional

3. FLC COMPUTATION APPROACHES

After image processing, the full-field surface strain contour maps were obtained for each frame. A sample major strain contour map (from stereo DIC) for a 50mm wide sample, representing the uniaxial tension strain path, is shown in Figure 5(a). This map was taken at the frame right before rupture, and it demonstrates how the test sample thinned down within its geometrical center (as desired for FLC

points extraction). In addition to the major strain map, a vertical section is drawn on the DIC correlated area and the Z-displacement along the section is plotted in Figure 5(b). The map shows that the Marciniak test sample deformed in-plane while growing out-of-plane to a height of ~16.6 mm. It is important to note that the entire deformation zone of the test sample stretched comparatively in-plane with a maximum variation of 0.15 mm between the thinned area and the surrounding region. This observation is critical to the 2D DIC error compensation method proposed in this work.

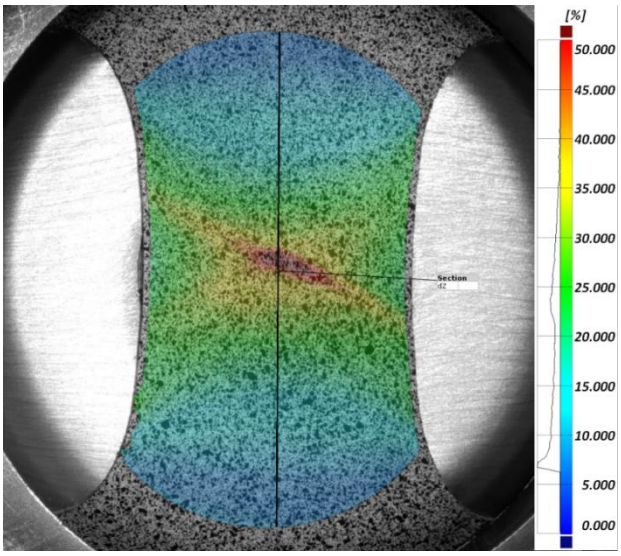

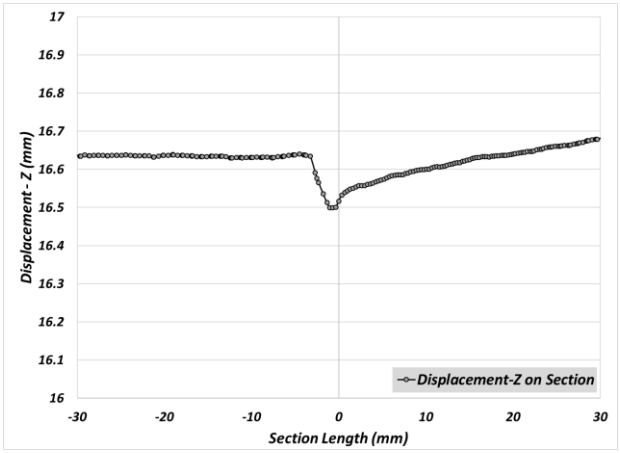

Figure 5. (a) Major strain contour map and a vertical section at the last frame before rupture on a 50 mm wide test sample; (b) Z-Displacement (mm) along the vertical section drawn on the test sample

3.1. ISO 12004-2 Standard Section-Based Method

The section-based method dictated by the ISO 12004-2 standard is a spatial method that is applied to the strain distributions in the last frame before rupture. In this method, five virtual sections (at least 3) are applied to the test sample surface perpendicular to the crack (for $\varepsilon_2 > 0$) and along the shaft direction (for $\varepsilon_2 < 0$) with a 2 mm spacing from each other (an example of this is shown in Figure 6). Each section results in one point on the FLC. Therefore, each sample generates 5 points (one per section), which are averaged to obtain the sample average. The average of all the sections coming from the repeats of the same geometry give the geometry average. From these sections, major and minor strain distributions (along the entire section length) are obtained and then fit to an inverse parabola within a window on both sides of the crack. The fitting windows are determined using the second derivative of strain values against their position on the section [15]. The true strain values on the parabolic fit at the position of the crack give the major and minor strain values that map as an FLC point on the formability diagram for the material. An example of this is demonstrated in Figure 7.

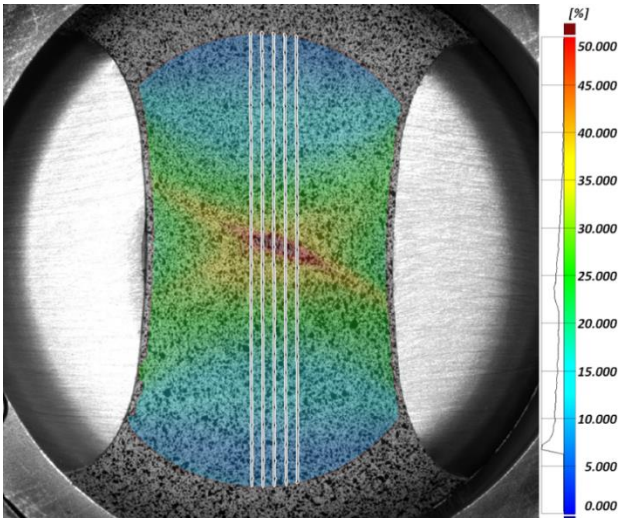

Figure 6. Major strain contour map and five virtual sections drawn on a 50 mm wide sample shown in Figure 5

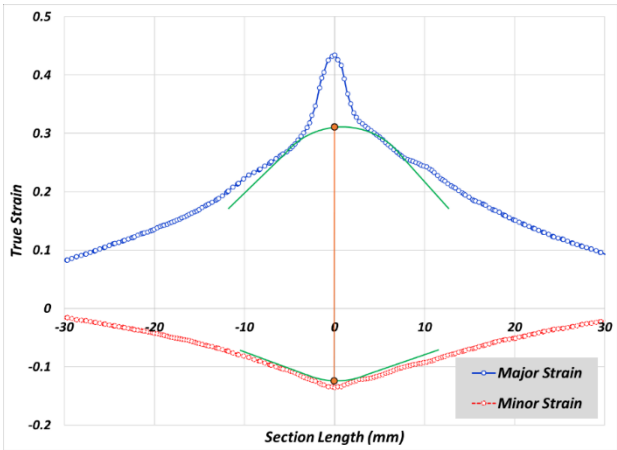

Figure 7. Major and minor strain values (and inverse parabolic fits) at a section across the crack on the 50mm wide sample that is shown in Figure 5

3.2. Linear Best Fit (LBF) Method

The LBF method for instability detection proposed by Volk and Hora in 2011 [14] is based on a time-dependent approach. This approach uses the rate of thinning of the material within a defined region of instable necking, which shows a sharp rise in thinning strains at the onset of instability compared to the surrounding region. There are different criteria used in the literature for the area selection. Volk and Hora [14] suggest a maximum thinning rate based selection where there should be a minimum of 7 to 15 subsets for a 1 mm grid and 5 to 10 elements for a 2 mm grid. In this study, the necking region is defined as the collection of all the subsets which have an effective strain value higher than 90% of the maximum effective strain on the sample in the last frame before rupture, as shown in Figure 8. The major (ε_1) and minor (ε_2) strain values averaged over the necking region are extracted for the entire deformation history, and thickness strain (ε_3) is calculated based on the volume constancy law, shown in eq. (1):

$$\varepsilon_1 + \varepsilon_2 + \varepsilon_3 = 0 \qquad (1)$$

Thinning rate (the first derivative of thinning) is then calculated and averaged over a moving fit window of 7 points to reduce the effect of noise. This calculation is performed over the frames that represent the last 4 mm of punch displacement before rupture. In this study, since the camera acquisition rate was set to 20 Hz, the total number of images selected for the LBF calculation is 160. Major, minor, and thinning strains, along with the thinning rate, are shown with respect to the punch displacement (within the last 4 mm) in Figure 9. The approach makes use of a stable line fit (linear fit over the punch displacement of -4 mm to -2 mm) and an instable line fit (linear fit over the last 7 points before rupture). The intersection of the two lines corresponds to the critical point in time when the instable necking is believed to have started, thus the major/minor strain values at this point are considered an FLC point.

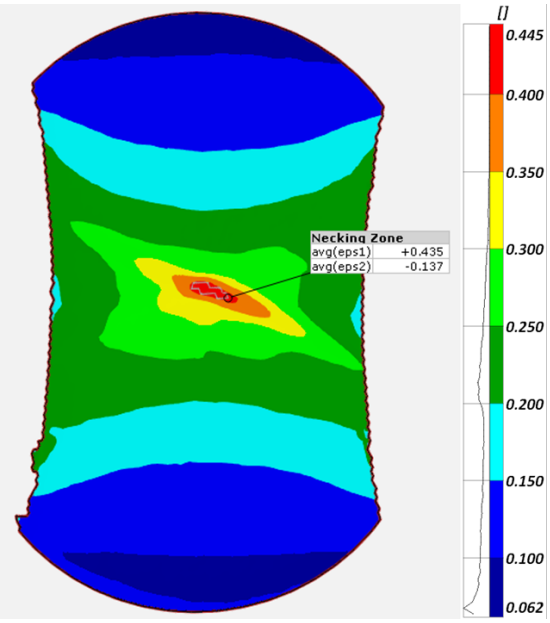

Figure 8. Effective strain contour map and necking zone selection on the 50mm wide sample

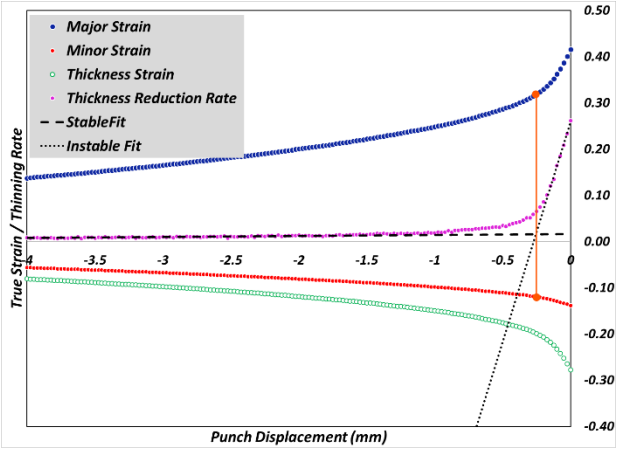

Figure 9. Necking zone strains and linear fitting lines for the LBF method plotted for the last 4 mm of the punch displacement for the 50mm wide sample shown in Figure 5

4. OUT-OF-PLANE ERROR COMPENSATION IN 2D DIC

Based on the working principle of a pinhole camera, an object is perceived as bigger when it is closer to the camera, and smaller when it is away from the camera. The measurements performed by a 2D DIC are prone to errors if the measuring distance between the camera and the test sample changes. When an FLC test sample is deformed and comes closer to the camera, as is the case here in Marciniak FLC testing, artificial positive strains are added to the actual strains; our objective is to remove these artificial strains.

Figure 10 shows a schematic of the Marciniak FLC test setup with 2D DIC. As explained in Section 3 and Figure 5(b), the Marciniak test is an in-plane test, i.e., the gauge area of the flat test sample deforms in-plane like an inverted cup, and the entire deformed plane moves closer to the camera. This means that the error in the 2D DIC measurements for Marciniak tests is systematic and similar for all the points within the deformation zone. Therefore, it can be quantified for each stage of deformation and can be separated from the actual strain measurements. It is theoretically derived that the artificial strain added to the measurements due to the out-of-plane translation of the sample is a ratio of change in measuring distance (Δz) and the initial measuring distance (z) [24]. The cup height (Δz) is a function of punch displacement and can be calculated using the punch speed and test time recorded by the DIC system, as given in eq. (2). The out-of-plane error in the measurements can be removed from the measured strains using eq. (3).

$$\Delta z = Punch\ Speed\ x\ Test\ Time \qquad (2)$$

$$\in (\%)_{corrected} = \in (\%)_{measured} - \frac{\Delta z}{z}(\%) \qquad (3)$$

In this study, the punch speed was 0.5 mm/s, which was multiplied by the test time (for each frame) to obtain the cup height or the out-of-plane translation Δz for that frame. The initial measuring distance of the 2D camera from the test sample plane is 450 mm (Table 1); using these two equations, the artificial strain was calculated for each frame and removed from the measurements.

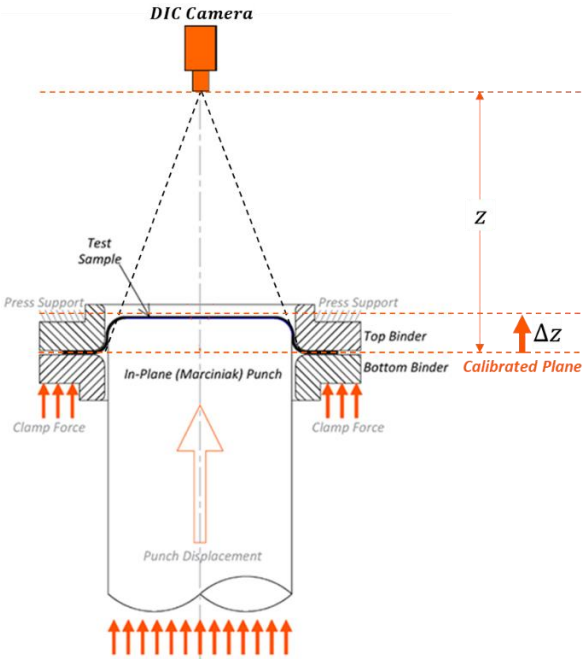

Figure 10. Schematic of the Marciniak FLC test setup with 2D DIC showing a deforming sample translating closer to the camera and away from the 2D DIC calibrated plane

5. EXPERIMENTAL RESULTS

Before presenting the results, it is important to note that in this study, the FLC generated by the stereo DIC is considered a benchmark, and the 2D DIC results are compared to it. Figure 11 shows an example of strain contour maps obtained from the two DIC systems for a particular 50mm test sample at the same timestamp. As noted, the major strain distribution across the entire sample looks very similar for the two DIC systems, when the legends of the two plots are set appropriately. This suggests that the strains in the 2D measurements have a positive offset compared to the stereo DIC strains, as expected due to the sample deforming towards the camera.

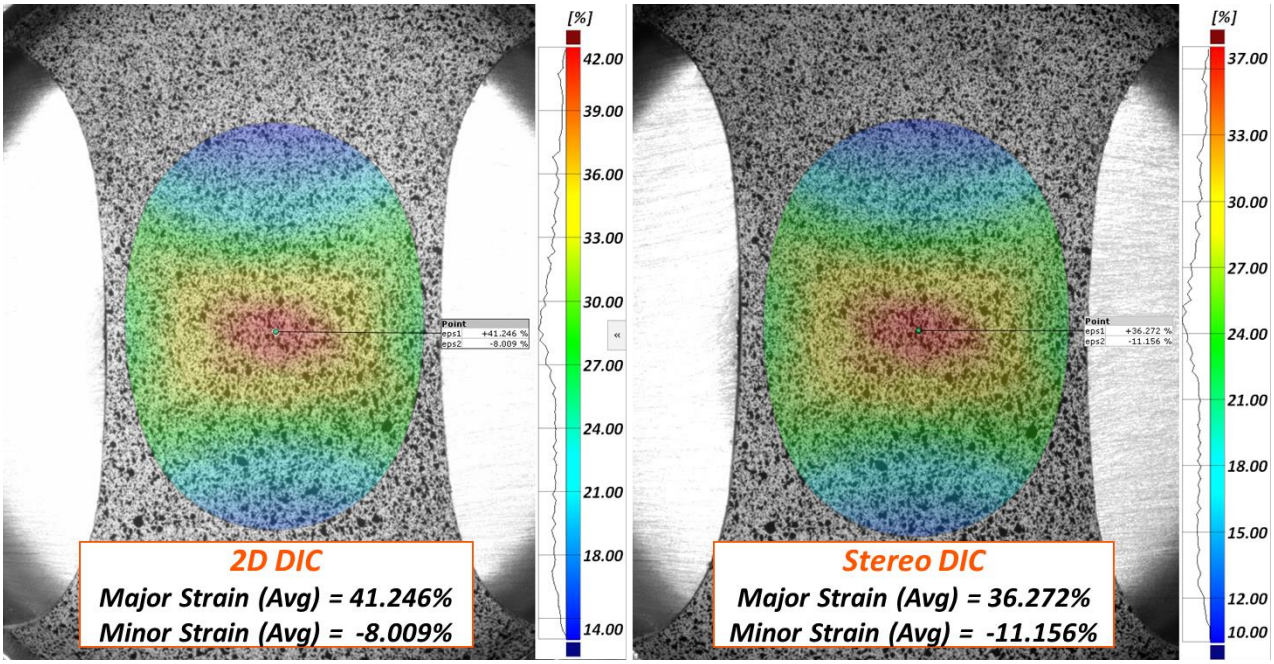

Figure 11. Major strain contour maps for a 50mm wide sample at the same timestamp obtained using 2D DIC and stereo DIC

5.1. FLC by the Section-Based Method

Following the steps outlined earlier in section 3.1, Figure 12 shows the resulting FLC points obtained from the two DIC systems. The two FLC curves are widely different; in general, the FLC points generated by the 2D DIC are shifted upwards and to the right when compared to those of the stereo DIC system. In other words, the FLC points obtained from the 2D DIC are higher in major strain and minor strain compared to the stereo DIC generated points. To investigate the reason behind the deviation, the major and minor strain profiles were extracted for a particular section, and a plot of that is shown in Figure 13. Both strain profiles extracted from the two DIC systems follow the same shape, with an upward offset of approximately 0.04 strains in the 2D DIC strains. Since the major strain and minor strain profiles have the same shape, the FLC point obtained by the inverse parabolic fit is also expected to offset by the same amount. After applying the correction outlined in section 4, and removing the artificial strains associated with out-of-plane translation, the corrected FLC points obtained by 2D DIC are plotted against stereo DIC results in Figure 14 and tabulated in Table 2. The FLC plots from the two DIC systems now overlap with a good agreement.

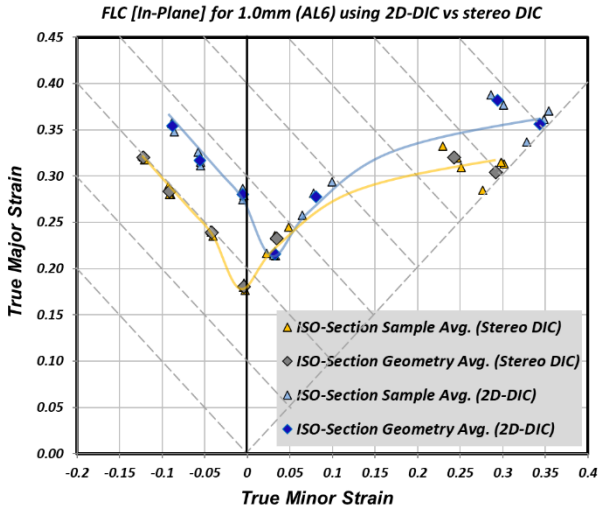

Figure 12. In-Plane FLCs for AL6 generated by the ISO section-based method using 2D DIC (before correction) and stereo DIC

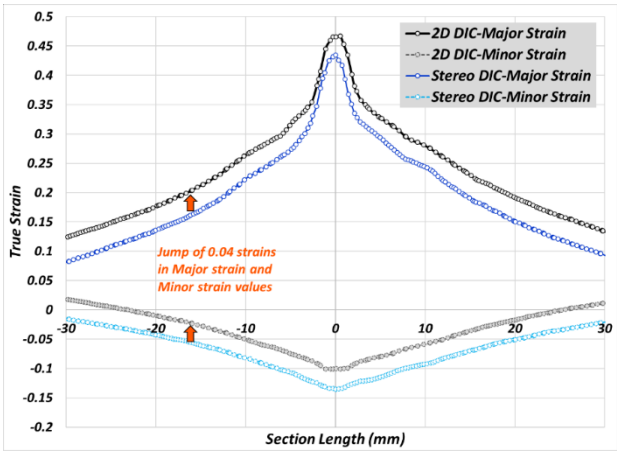

Figure 13. Major and minor strain section distributions for a 50mm wide test sample based on 2D DIC and stereo DIC

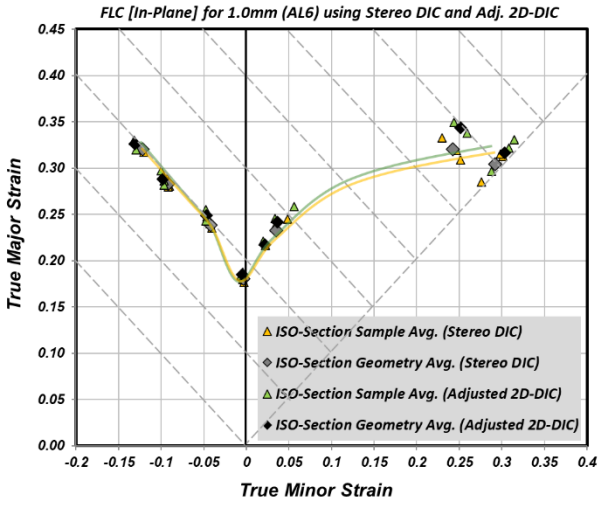

Figure 14. In-Plane FLCs for AL6 generated by the ISO section-based method using 2D DIC (after correction) and stereo DIC

5.2. FLC by the LBF Method

The LBF method is a time-dependent approach based on the entire major-minor strain evolution history in the last 4 mm of punch travel, unlike the section-based method which is dependent only on the last frame before rupture. Also, the procedure involves fitting of a non-linear quantity (thinning reduction rate). Therefore, the correction outlined here can't be applied directly on the critical FLC point and instead needs to be done on the major-minor strain pairs for each frame within the last 4 mm range of punch travel. After applying the correction, the compensated major and minor strains were used to calculate the thinning strain, then thinning reduction rate, and finally fits to the stable and unstable regions were obtained per the procedure. The FLCs generated by the 2D DIC system using the LBF method, before and after correction, are plotted against those obtained by the stereo DIC system in Figure 15 and Figure 16 and tabulated in Table 3. Again, the corrected FLC points generated by 2D DIC overlap with a very good agreement to the stereo DIC points.

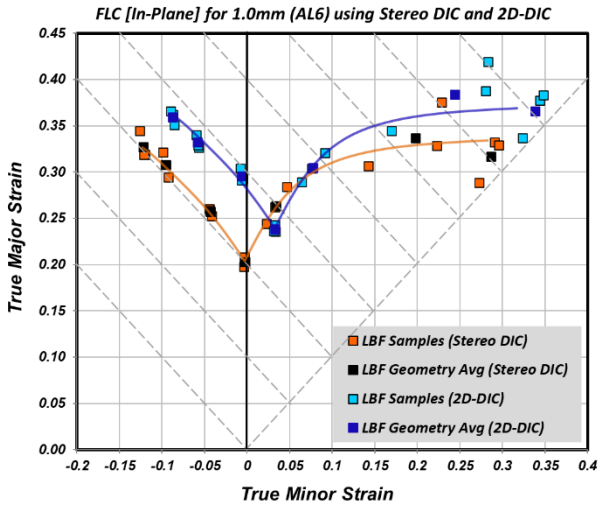

Figure 15. In-Plane FLCs for AL6 generated by the LBF method using 2D DIC (before correction) and stereo DIC

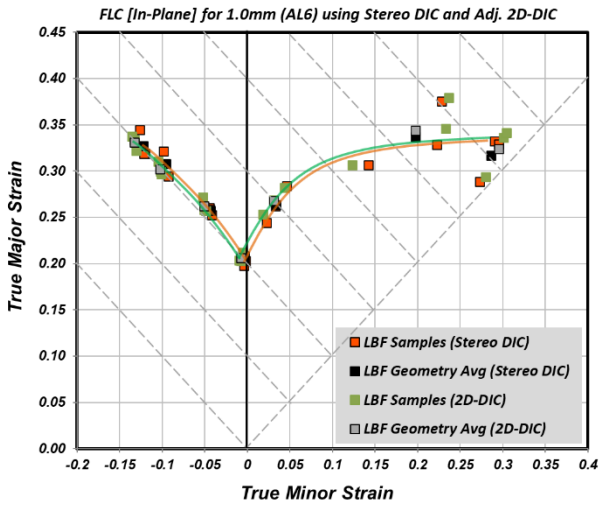

Figure 16. In-Plane FLCs for AL6 generated by the LBF method using 2D DIC (after correction) and stereo DIC

6. DISCUSSION

The proposed method for correcting 2D DIC strain measurement for determining FLC points is simple, effective, and material-independent for Marciniak testing of any sheet metal alloy under the given considerations. Although the global deformation in a Marciniak test is in-plane, there is some out-of-plane thinning in the material before rupture [27]. Also, it is

published in the literature [28] that the bending resistance of the metal usually causes a slight crown to develop in the center of the Marciniak cup. It can be argued that this out-of-plane thinning and crown is not accounted for in the correction approach. However, it is mathematically seen that the effect of these local deformations is insignificant. Example: for a 1mm thick sheet metal, a 50% thinning before rupture leads to an out-of-plane Δz of 0.5 mm leading to an error of less than 0.001 strains (measured on a 450mm calibrated distance). Therefore, the errors in the planar tests are not noticeable.

The proposed method is shown to work for both the ISO 12004-2 section-based spatial method and the time-dependent LBF method. However, the procedure can be extended to other spatial, time-dependent, and hybrid methods. Due to the inability of the 2D DIC to perceive any changes in the depth dimension, the method would not work on a specific class of FLC computation algorithms that work on the change in sheet curvature for the identification of the onset of instable necking [18], [19].

Table 2. Section method based FLC points (average) for AL6 measured by stereo DIC, 2D DIC (before correction) and 2D DIC (after correction)

FLC Point	Stereo DIC		2D DIC (Before Correction)		2D DIC (After Correction)	
	Major Strain	Minor Strain	Major Strain	Minor Strain	Major Strain	Minor Strain
1	0.320	-0.122	0.354	-0.088	0.326	-0.131
2	0.283	-0.092	0.317	-0.056	0.288	-0.098
3	0.239	-0.042	0.280	-0.005	0.248	-0.047
4	0.180	-0.004	0.216	0.033	0.185	-0.005
5	0.232	0.035	0.278	0.080	0.242	0.036
6	0.320	0.243	0.382	0.294	0.343	0.252
7	0.304	0.292	0.356	0.344	0.316	0.303

Table 3. LBF method based FLC points (average) for AL6 measured by stereo DIC, 2D DIC (before correction) and 2D DIC (after correction)

FLC Point	Stereo DIC		2D DIC (Before Correction)		2D DIC (After Correction)	
	Major Strain	Minor Strain	Major Strain	Minor Strain	Major Strain	Minor Strain
1	0.327	-0.122	0.360	-0.088	0.331	-0.133
2	0.308	-0.096	0.332	-0.058	0.302	-0.103
3	0.257	-0.043	0.296	-0.006	0.262	-0.050
4	0.203	-0.003	0.238	0.032	0.206	-0.007
5	0.263	0.034	0.304	0.077	0.268	0.031
6	0.337	0.198	0.384	0.244	0.344	0.198
7	0.317	0.286	0.366	0.338	0.324	0.295

7. CONCLUSIONS

This paper offers a simplistic method for enabling Forming Limit Curve (FLC) experimental determination for sheet metal alloys using a low-cost 2D Digital Image Correlation (DIC) system. The method was tested on Marciniak tests performed on a 1 mm thick aluminum alloy (AL6) using a custom setup that enabled simultaneous measurements of strains using stereo DIC and 2D DIC systems. The FLC points were determined using two popular and well-accepted methods; the ISO 12004-2 section-based method and the LBF time-dependent method. The FLCs obtained after the application of the proposed correction to 2D DIC strains showed a good agreement with those FLCs obtained by a stereo DIC system.

The results prove that an FLC for a sheet metal alloy can be accurately determined using a single camera DIC system. By no means does this work encourage replacing stereo DIC systems with 2D DIC systems; rather, the objective here is to enable greater and faster adoption of DIC in budget-constrained settings to bring the advantages of using optical metrology over traditional FLC determination methods. This is to promote additional formability work by academic institutions by reducing the requirements for heavy investments in stereo DIC systems or even 2D DIC systems with telecentric lenses.

The proposed method of strain correction is intended only for Marciniak tests; the correction method would change for out-of-plane FLC Nakajima tests, and that will be covered in another publication.

REFERENCES

[1] G. M. Goodwin, "Application of Strain Analysis to Sheet Metal Forming Problems in the Press Shop," *SAE Technical Papers*, Feb. 1968, doi: 10.4271/680093.

[2] S. KEELER and B. WG, "RELATIONSHIP BETWEEN LABORATORY MATERIAL CHARACTERIZATION AND PRESS-SHOP FORMABILITY".

[3] Z. Marciniak and K. Kuczyński, "Limit strains in the processes of stretch-forming sheet metal," *Int J Mech Sci*, vol. 9, no. 9, pp. 609–620, Sep. 1967, doi: 10.1016/0020-7403(67)90066-5.

[4] K. Nakazima, Toshio Kikuma, and Kaname Hasuka, "Study on the formability of steel sheets," *YAWATA TECH REP, SEPT*, vol. 264, pp. 8517–8530, 1968.

[5] L. Huang and M. Shi, "Determination of the Forming Limit Curve Using Digital Image Correlation - Comparison of Different Approaches to Pinpoint the Onset of Localized Necking," *SAE Technical Papers*, vol. 2017-March, no. March, Mar. 2017, doi: 10.4271/2017-01-0301.

[6] A. Agha and F. Abu-Farha, "Numerical implementation and validation of a viscoelastic-plastic material model for predicting curing induced residual stresses in adhesive bonded joints," *Int J Adhes Adhes*, vol. 118, p. 103195, Oct. 2022, doi: 10.1016/J.IJADHADH.2022.103195.

[7] R. Esmaeilpour, H. Kim, T. Park, F. Pourboghrat, A. Agha, and F. Abu-Farha, "Effect of hardening law and process parameters on finite element simulation of single point incremental forming (SPIF) of 7075 aluminum alloy sheet," *Mechanics & Industry*, vol. 21, no. 3, p. 302, 2020, doi: 10.1051/MECA/2020019.

[8] M. Nazzal, M. Alkhader, A. Agha, F. Abu-Farha, Z. Ali, and W. AlDamaty, "Wrinkling suppression in thin membranes using designed geometrical features," *https://doi.org/10.1177/09544062221101976*, vol. 236, no. 19, pp. 10163–10174, May 2022, doi: 10.1177/09544062221101976.

[9] A. Agha and F. Abu-Farha, "Experimental methods to capture curing induced effects in adhesive bonded joints," *Int J Adhes Adhes*, vol. 104, p. 102735, Jan. 2021, doi: 10.1016/J.IJADHADH.2020.102735.

[10] A. Agha and F. Abu-Farha, "Advanced Anti-Buckling Device Coupled with Real-Time Digital Image Correlation for Complex Cyclic Tension-Compression Testing of Lightweight Materials," *Evaluation of Existing and New Sensor Technologies for Fatigue, Fracture, and Mechanical Testing*, pp. 40–54, Aug. 2022, doi: 10.1520/STP163820210045.

[11] J. Hu, "Characterization and Modeling of Deformation, Springback, and Failure in Advanced High Strength Steels (AHSSs)," *All Dissertations*, Dec. 2016, Accessed: Dec. 02, 2022. [Online]. Available: https://tigerprints.clemson.edu/all_dissertations/1840

[12] "ISO 12004-2:2021 - Metallic materials — Determination of forming-limit curves for sheet and strip — Part 2: Determination of forming-limit curves in the laboratory".

[13] G. Huang, S. Sriram, and B. Yan, "Digital image correlation technique and its application in forming limit curve determination," in *Proceedings of the IDDRG 2008 International Conference*, 2008, pp. 16–18.

[14] W. Volk and P. Hora, "New algorithm for a robust user-independent evaluation of beginning instability for the experimental FLC determination", doi: 10.1007/s12289-010-1012-9.

[15] W. Hotz, M. Merklein, A. Kuppert, H. Friebe, and M. Klein, "Time Dependent FLC Determination Comparison of Different Algorithms to Detect the Onset of Unstable Necking before Fracture," *Key Eng Mater*, vol. 549, pp. 397–404, 2013, doi: 10.4028/WWW.SCIENTIFIC.NET/KEM.549.397.

[16] M. Merklein, A. Kuppert, and M. Geiger, "Time dependent determination of forming limit diagrams," *CIRP Annals*, vol. 59, no. 1, pp. 295–298, Jan. 2010, doi: 10.1016/J.CIRP.2010.03.001.

[17] A. J. Martínez-Donaire, F. J. García-Lomas, and C. Vallellano, "New approaches to detect the onset of localised necking in sheets under through-

thickness strain gradients," *Mater Des*, vol. 57, pp. 135–145, May 2014, doi: 10.1016/J.MATDES.2014.01.012.

[18] J. Min, T. B. Stoughton, J. E. Carsley, and J. Lin, "An improved curvature method of detecting the onset of localized necking in Marciniak tests and its extension to Nakazima tests," *Int J Mech Sci*, vol. 123, pp. 238–252, Apr. 2017, doi: 10.1016/J.IJMECSCI.2017.02.011.

[19] K. Wang, J. E. Carsley, B. He, J. Li, and L. Zhang, "Measuring forming limit strains with digital image correlation analysis," *J Mater Process Technol*, vol. 214, no. 5, pp. 1120–1130, May 2014, doi: 10.1016/J.JMATPROTEC.2014.01.001.

[20] J. Min, T. B. Stoughton, J. E. Carsley, and J. Lin, "Comparison of DIC Methods of Determining Forming Limit Strains," *Procedia Manuf*, vol. 7, pp. 668–674, Jan. 2017, doi: 10.1016/J.PROMFG.2016.12.099.

[21] X. Chen, N. Xu, X. Xie, L. Smith, and L. Yang, "Forming Limit Measurement Using a Multi-Sensor Digital Image Correlation System," *SAE Technical Papers*, vol. 2, Apr. 2013, doi: 10.4271/2013-01-1423.

[22] V. Novák, M. Valeš, F. Tatíček, J. Šanovec, and L. Chrášťanský, "The effect of strain rate on position of forming limit curve," *METAL 2019 - 28th International Conference on Metallurgy and Materials, Conference Proceedings*, pp. 450–454, 2019, doi: 10.37904/METAL.2019.825.

[23] S. B. Kim, H. Huh, H. H. Bok, and M. B. Moon, "Forming limit diagram of auto-body steel sheets for high-speed sheet metal forming," *J Mater Process Technol*, vol. 211, no. 5, pp. 851–862, May 2011, doi: 10.1016/J.JMATPROTEC.2010.01.006.

[24] M. A. Sutton, J. H. Yan, V. Tiwari, H. W. Schreier, and J. J. Orteu, "The effect of out-of-plane motion on 2D and 3D digital image correlation measurements," *Opt Lasers Eng*, vol. 46, no. 10, pp. 746–757, Oct. 2008, doi: 10.1016/J.OPTLASENG.2008.05.005.

[25] B. Pan, L. Yu, and D. Wu, "High-accuracy 2D digital image correlation measurements using low-cost imaging lenses: implementation of a generalized compensation method," *MeScT*, vol. 25, no. 2, p. 025001, Feb. 2014, doi: 10.1088/0957-0233/25/2/025001.

[26] B. Pan, L. Yu, and D. Wu, "High-Accuracy 2D Digital Image Correlation Measurements with Bilateral Telecentric Lenses: Error Analysis and Experimental Verification," *undefined*, vol. 53, no. 9, pp. 1719–1733, Nov. 2013, doi: 10.1007/S11340-013-9774-X.

[27] A. Agha, "Effectiveness of 2D Digital Image Correlation in Capturing the Fracture Behavior of Sheet Metal Alloys," *SAE International Journal of Materials and Manufacturing*, vol. 16, no. 2, Dec. 2022, doi: 10.4271/05-16-02-0009.

[28] J. Min, T. B. Stoughton, J. E. Carsley, and J. Lin, "Compensation for process-dependent effects in the determination of localized necking limits," *Int J Mech Sci*, vol. 117, pp. 115–134, Oct. 2016, doi: 10.1016/J.IJMECSCI.2016.08.008.